ELSEVIER

Journal of Photochemistry and Photobiology A: Chemistry 103 (1997) 1–9

Journal of PHOTOCHEMISTRY AND PHOTOBIOLOGY A:CHEMISTRY

Energy transfer and energy pooling from Ba[6s5d($^3D_{1,2,3}$)] generated following pulsed dye-laser excitation at $\lambda = 553.5$ nm {Ba[6s6p($^1P_1$) ← Ba[6s^2($^1S_0$)]} and monitored by time-resolved atomic emission from Ba[6s5d($^1D_2$)], Ba[6s6p($^3P_1$)] and Ba[6s6p($^1P_1$)] Part I

S. Antrobus, D. Husain *, Jie Lei

Department of Chemistry, University of Cambridge, Lensfield Road, Cambridge CB2 1EW, UK

Received 1 July 1995; accepted 1 October 1996

Abstract

We present a kinetic study of Ba[6s5d(^3D_J)], 1.151 eV above the 6s^2($^1S_0$) ground state ($J=1$, 1.120, $J=2$, 1.143, $J=3$, 1.190 eV). This was generated indirectly following the initial pulsed dye-laser excitation of atomic barium vapour at elevated temperature at $\lambda = 553.5$ nm {Ba[6s6p($^1P_1$)] ← Ba[6s^2($^1S_0$)]} in the presence of helium buffer gas in a slow flow system kinetically equivalent to a static system. The ^3D_J state was subsequently populated by various emission and collisional process from Ba($^1P_1$), including cascading via Ba[6s6p(^3P_J)] which is generated in this system. Direct monitoring via emission in the time-domain from Ba[6s5d($^3D_1$)] → Ba[6s^2($^1S_0$)] + $h\nu$ ($\lambda = 1106.9$ nm) using an interference filter and a new long wavelength response tube (S21) operating in this wavelength region did not prove sufficiently sensitive. Time-resolved emission measurements in the long-time regime (ca. 3 ms) at $\lambda = 791.1$ nm {Ba[6s6p($^3P_1$)] → Ba[6s^2($^1S_0$)]} and $\lambda = 877.4$ nm {Ba[6s5d($^1D_2$)] → Ba[6s^2($^1S_0$)]} were made following collisional excitation of Ba(^3D_J) to the ^3P_J and $^1D_2$ state by He and Ba and, in turn, used to monitor the decay of the ^3D_J state itself. Further, the long-time emission (ca. 1.5 ms) at $\lambda = 553.5$ nm {Ba[6s6p($^1P_1$)] → Ba[6s^2($^1S_0$)]} ($\tau_e = 8.37 \pm 0.38$ ns) resulting from excitation at this wavelength was also employed to monitor Ba(^3D_J) following energy pooling to this state accompanying the Ba(^3D_J) + Ba(^3D_J) self-annihilation. The detailed mechanism for this system was considered quantitatively in terms of the optical and collisional processes for populating the emitting states employing both the form of time profiles and integrated atomic emission intensities. The results are shown to be quantitatively in accord with the proposed mechanisms for population and excitation and indicate that these time-resolved emission measurements from states resulting from energy transfer and energy pooling act as spectroscopic markers for Ba(^3D_J). © 1997 Elsevier Science S.A. All rights reserved.

Keywords: Excited barium atoms; Ba(^{3}D); Laser excitation; Energy transfer; Energy pooling; Spectroscopic markers

1. Introduction

Considerable emphasis on the experimental and theoretical investigation of the collisional behaviour of electronically excited alkaline earth atoms, a subject which has been regularly reviewed on account of the range of studies carried out both using molecular beams and the time-domain following laser excitation [1–4], has been directed towards optically metastable states where collisional removal can compete significantly with spontaneous emission at normal pressures. As far as measurements in the time-domain using pulsed laser investigations are concerned, such low lying states of Mg, Ca and Sr have been and are directly accessible for kinetic studies by direct excitation into the long-lived states [1–4]. By contrast, the metastable states of barium, namely, Ba[6s5d($^3D_{1,2,3}$)] (1.120, 1.143 and 1.190 eV, respectively [5]) and Ba[6s5d($^1D_2$)] (1.413 eV [5]) have normally been populated by processes such as cascading fluorescence, stimulated emission, stimulated Raman scattering and collisional quenching processes following initial laser excitation via a strongly allowed transition to a higher lying state. Similarly, the reported and quoted radiative lifetimes of these states vary considerably in the literature, for example, earlier values include τ_e{Ba[6s5d(^3D_J)]} = from ca. 100 μs to ≥ 1 ms [6,7] and τ_e[Ba[6s5d($^1D_2$)]] ≤ 31.3 μs [8,9]. It may immediately be seen that collisional processes under-

* Corresponding author.

1010-6030/97/$17.00
PII S1010-6030(96)04519-4

gone by Ba[6s5d(^3D_J)] will take place on a completely different time scale to those which follow the initial production of Ba[6s6p($^1P_1$)], employed in this system for the eventual production of the ^3D_J state, where the mean radiative lifetime is much shorter ($\tau_c = 8.37 \pm 0.38$ ns [10]). The present paper thus describes energy transfer and energy pooling processes in the long time-domain resulting from Ba[6s5d(^3D_J)], generated initially via the laser production of Ba[6s6p($^1P_1$)], where the time-resolved emission from the states higher lying than the ^3D_J state and resulting from these collisional processes are used as spectroscopic markers for the Ba(^3D_J) state itself.

The generation of Ba[6s5d(^3D_J)] and Ba[6s5d($^1D_2$] following pulsed laser generation of Ba[6s6p($^1P_1$)] from barium vapour at $\lambda = 535.5$ nm {Ba[6s6p($^1P_1$)] ← Ba[6s^2($^1S_0$)]} is well established. A range of detailed measurements have been reported on branching ratios into Ba($^1D_2$) and Ba(^3D_J) following laser excitation at $\lambda = 535.5$ nm including emission and collisional processes [11–17]. Emission from Ba[6s6p($^1P_1$)] and Ba[6s6p($^3P_1$)] to Ba[5s5d(^3D_J)] populates the $J = 1$ and 2 levels on the basis of an electric dipole-allowed transition ($\Delta J = 0, \pm 1$) for (j,j) coupling though there will, of course, be subsequent collisional mixing with the ^3D_J spin–orbit manifold. This can be seen in considerable detail from the measurements of Ehrlacher and Huennekens [18] who describe rapid spin–orbit mixing in Ba($^3D_{1,2,3}$) by collisions with Ar, N_2 and Ba itself following stimulated emission or stimulated Raman scattering in Ba($^3D_{1,2}$) subsequent to the generation of Ba[6s6p($^3P_1$)] by direct laser excitation from the ground state at $\lambda = 791.1$ nm. Collisional quenching of Ba[6s6p($^1P_1$)] by rare gases has been shown to yield exclusively Ba[6s6p($^3P_2$)] [19,20] in 'pump-and-probe' measurements and molecular beams, with no production of Ba($^1D_2$) or Ba(^3D_J) though some evidence for the production of Ba[6s6p($^3P_1$)] has been reported from molecular beam measurements [21] with subsequent rapid emission into the ^3D_J manifold [22]. The overall mean radiative lifetimes of the individual spin–orbit states of Ba[6s6p($^3P_{0,1,2}$)] are short ($^3P_0$, 2.4 μs [23]; $^3P_1$, 1.2 ± 0.1 μs [23–25]; $^3P_2$ 1.3 μs [23]) and thus, within such lifetimes, the system has relaxed either to the $^1S_0$ ground state or to the mestastable D states for monitoring in the long-time regime. The mean radiative lifetime of Ba(6s5d($^1D_2$)] is ≤31.3 μs [8,9] and, indeed, the $^1D_2$ state has been generated initially via laser excitation initially to the 6p'($^1P_1$) state at $\lambda = 350.1$ nm and monitored by atomic absorption spectroscopy to this state at $\lambda = 582.6$ nm on time-scales of this magnitude and, of course, considerably shorter (≥2.5 μs) for characterising collisional quenching data of Ba($^1D_2$) with N_2, CO, H_2 and D_2 [8]. Light-induced drift measurements on this metastable state following initial laser excitation to Ba[6s6p($^1P_1$)] at $\lambda = 553.5$ nm has also been reported [26].

The average mean radiative lifetime of Ba[6s5d(^3D_J)] is much longer than the $^1D_2$ state (ca. 100 μs [6], ≥1 ms [7]) and hence the precursor to emission from a higher lying state in the long-time regime can be ascribed as originating on a collisional basis from the ^3D state, which is the content of this paper. Whitkop and Wiesenfeld [27] have monitored Ba($^3D_{1,2,3}$) by time-resolved atomic absorption spectroscopy following initiation excitation to the 6p5s($^1P_1$) state at $\lambda = 553.5$ nm in order to characterise collisional quenching rate data particularly by Ba itself. Solarz and Johnson [6] have monitored the chemical products of the reaction of Ba(^3D_J) following initial excitation to Ba[6s6p($^3P_1$)] at $\lambda = 791.4$ nm by laser-induced fluorescence in a beam system. Chemiluminescence from diatomic products of various atomic abstraction reactions of Ba(^3D_J) in beam–gas measurements, including specificity in the spin–orbit components using optical excitation, have employed the initial generation of the ^3D state by low voltage discharge [28,29]. Energy pooling to higher lying atomic states arising from the self-annihilation between Ba(^3D_J) + Ba(^3D_J) has been reported hitherto [30] and this, together with emission from higher lying states of atomic barium resulting from energy transfer, will be described in this paper and quantitatively demonstrated as spectroscopic markers for the ^3D_J state. Time-resolved emissions, including quantitative measurements of integrated atomic intensities, are described, and compared in detail for the energy transfer and energy pooled states including a detailed consideration of the excitation and transfer processes. Overall, emissions from these higher lying states are shown to provide a quantitative basis for studying Ba(^3D_J) in the time-domain.

2. Experimental

The general experimental arrangement for monitoring atomic resonance fluorescence, energy pooling and energy transfer emission from atomic barium in the time-domain following pulsed dye-laser excitation was similar to that described in our recent investigations on chemical reactions of Sr(5^3P_J) [31] and energy pooling on Sr(5^3P_J) [32,33] with a number of modifications to the isolation and detection systems for the various transitions of atomic barium. Ba[6s6p($^1P_1$)] was generated using the second harmonic (532 nm) of a Nd:YAG primary laser (10 Hz) (J.K. Lasers, System 2000) to pump a dye-laser (Rhodamine chloride 590, typically 1.0×10^{-4} M in methanol, Exciton) operating at $\lambda = 553.55$ nm (Ba[6s6p($^1P_1$)] ← Ba[6s^2($^1S_0$)]. Barium vapour at various elevated temperatures [34] was thus excited to the $^1P_1$ state at the resonance wavelength in the presence of excess helium buffer gas. The following atomic transitions were monitored as a function of time both in the 'short-time region' and the 'long-time regime' (see later): Ba[6s6p($^1P_1$)] → Ba[6s^2($^1S_0$)], $\lambda = 553.5$ nm; Ba[6s6p($^3P_1$)] → Ba[6s^2($^1S_0$)], $\lambda = 791.1$; Ba[6s5d($^1D_2$)] → Ba[6s^2($^1S_0$)], $\lambda = 877.4$ nm). This involved the previous systems we have described including both optical isolation using monochromators [31–33] and also, here, interference filters for greater light throughput. Two monochromator–

photomultiplier systems were employed. (i) The first involved a photomultiplier tube with an S20 response (E.M.I., 9797B) whose gain (G) can sensibly be fitted to the form $\ln(G/\text{arb. units}) = 8.7 \ln(V/\text{V}) - 54.4$ [35]. This was combined with a small high throughput 'Minichrom' monochromator (MC1-02-10288, Fastie-Ebert mounting; $f/4$; focal length 74 mm; range 200–800 nm; grating mm square; 1800 lines per mm). The wavelength response of the photomultiplier–grating combination was calibrated against a quartz-halogen lamp which had previously been calibrated against a spectral radiometer (International Light Inc., USA, IL783). This yielded two maxima in the sensitivity response curve, one at ca. 440 nm and the other at ca. 510 nm, representing the expected combination of the blaze of the grating for the former and the maximum of the photomultiplier tube response for the latter. (ii) The second monochromator–photomultiplier system employed the new infrared sensitive photomultiplier tube (Hamamatsu R632-S1 response) that we have described previously in our investigations at long wavelength on atomic strontium at $\lambda = 1124.1$ nm $\{Sr[5s6s(^1S_0)] \rightarrow Sr[5s5p(^1P_1)]\}$ [33]. This is a 12-dynode device with a photocathode material of Ag–O–Cs and a sensitivity range of ca. 400–1200 nm. The wavelength response shows a bimodal distribution, with maxima at ca. 310 and 800 nm, and a trough at 450 nm. Whilst the overall sensitivity is relatively low, the quantum efficiency being little more than 1% at 310 nm and 0.1% at 1000 nm, the operational wavelength range is large. The gain (G) of the tube can sensibly described by the form $\ln G = 8.48 \ln(V/\text{V}) - 47.28$ ($\gamma = 0.998$) from the commercial gain characteristic. This was combined with a further high throughput compact monochromator (Speirs Robertson GM 100; aperture ratio f 4.7; fixed slits 0.5 mm) that included a grating with optical sensitivity at long wavelength (Speirs Robertson GM 100-5; range 350–1100 nm; 590 grooves per mm; blaze 500 nm). The wavelength response of this photomultiplier–grating combination was again calibrated using a quartz halogen lamp and the above spectral radiometer. The double maxima in the wavelength response of the p.m. tube coupled with the blaze of the grating subsequently yields a curve with a single maximum at λ = ca. 700 nm (arbitrary value 100). The response at, say, $\lambda = 1100$ nm is *not* zero but ca. 0.3 on this arbitrary scale and the response is approximately flat at this value to $\lambda = 1200$ nm. This can be offset by the increase in gain of the p.m. tube with voltage (see earlier) which, whilst necessarily involving scatter from noise in the tube, is significantly reduced by signal averaging. The combination of the wavelength response of the p.m. grating systems and the gain characteristics of the p.m. tubes with voltage are employed in determining integrated atomic intensities from decay profiles. The forms of the decay profiles themselves are, of course, independent of these calibrations.

Measurements on the long wavelength emissions associated with emission from the $^1D_2$ and ^3D_J states ($Ba[6s5d(^1D_2)] \rightarrow Ba[6s^2(^1S_0)]$, $\lambda = 877.4$ nm; $Ba[[6s5d(^3D_1) \rightarrow Ba[6s^2(^1S_0)]$, $\lambda = 1106.9$ nm) were also investigated using interference filters in order to improve light collection. As will be seen later, in the latter case, the measurements were not successful on account of the low sensitivity of the R632-S1 tube, coupled with the density of $Ba(^3D_J)$. The two interference filters were centred at $\lambda = 877.5$ nm (Speirs Robertson, FWHM 17 nm, max. trans. 58%) and $\lambda = 1111$ nm (Speirs Robertson, FWHM 10 nm, max. trans. 56%). For the parity forbidden transition at 877.4 nm, this is clearly close to the maximum transmission of the interference 877.5 nm filter; the longer wavelength filter was used at 1106.9 nm where the transmission is ca. 40%. The former filter was used with the S20 p.m. tube (E.M.I., 9797B) and the latter, with the S21 tube (R632). Similar photomultiplier gating circuitry was used to eliminate the effect of scattered light from the laser initiation pulse with all detection systems described here and follows that reported in previous investigations [31–33]. Typically, a reverse pulse of 100 V of varied duration was applied across the 5th and 7th dynodes of the photomultiplier chain, during which the laser pulse was applied, and yielding an attenuation of ca. 100:1 for both p.m. tubes.

Digitised data capture of complete profiles was employed in contrast to the earlier use of boxcar integration. The decay profiles were thus captured with a double-channel transient digitiser ('Digital Storage Adapter', Thurlby DSA 524) interfaced to a computer. 255 decay profiles were captured and averaged as were 255 background profiles before transfer and subtraction for computerised analysis. Measurements of the integrated atomic intensities were calculated from the recorded decay profiles coupled with calibration of the response of the optical systems and the photomultiplier gain characteristics. The materials (Ba (Aldrich Chemicals), He) were employed essentially as described in the previous investigations on analogous measurements on atomic strontium [31–33].

3. Results and discussion

Fig. 1(a) gives an example of the digitised output indicating the decay of the time-resolved atomic emission at

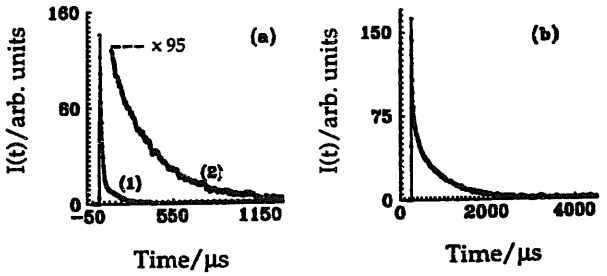

Fig. 1. Examples of the digitised output showing the decay of the time-resolved atomic emission at (a) $\lambda = 553.5$ nm $\{Ba[6s6p(^1P_1)] \rightarrow Ba[6s^2(^1S_0)]$ $T = 880$ K and (b), $\lambda = 877.4$ nm $\{Ba[6s5d(^1D_2)] \rightarrow Ba[6s^2(^1S_0)]$ $T = 900$ K following the pulsed dye-laser excitation of atomic barium at $\lambda = 553.5$ nm $\{Ba[6s6p(^1P_1)] \leftarrow Ba[6s^2(^1S_0)]\}$ in the presence of helium buffer gas ($P_{He} = 80$ Torr).

$\lambda = 553.5$ nm {Ba[6s6p($^1P_1$)] → Ba[6s^2($^1S_0$)]} following the resonance excitation of ground state atomic barium at elevated temperatures in the presence of excess helium buffer gas. This employed the 'Minichrom system' with the p.m. tube of the S20 response (E.M.I. 9797B). The emission is seen to comprise two components, a short component which arises from fluorescence ($\tau_c(6^1P_1) = 8.37 \pm 0.38$ ns [10]) and laser scattering, and a long-time, much weaker component which arises from energy pooling (see later) between two Ba[6s5d(^3D_J)] atoms. The actual lifetime of the short-time component at this wavelength results principally from the RC component in the fast-settling operational amplifier employed in the current-to-voltage converter [36] to amplify the photoelectric signals. Fig. 1(b) shows the parity forbidden emission at $\lambda = 877.4$ nm {Ba[6s5d($^1D_2$)] → Ba[6s^2($^1S_0$)]} following excitation at $\lambda = 553.5$ nm. This study of this emission employed the interference filter for this wavelength ($\lambda = 877.5$ nm) coupled with the R632 p.m. tube (Hamamatsu S1 response) for greater light gathering power of this weak emission. It was difficult to detect using even a small monochromator though it was observed by that method of optical isolation but not strongly enough for constructing decay profiles. The short wavelength component may reflect the estimates of $\tau_c(^1D_2)$ (≤ 31.3 μs [4,8,9]) and the RC response of the electronic detection system [36]. The long-time component may be seen to arise from energy transfer between Ba(^3D_J) + He and Ba. The rate of this collisional excitation process may be seen from the data reported for the reverse collisional relaxation processes:

$$\text{Ba}[6s5d(^1D_2)] + \text{He} \rightarrow \text{Ba}[6s5d(^3D_J)] + \text{He} \quad k_1^{\text{He}} \qquad (1)$$

$$\text{Ba}[6s5d(^1D_2)] + \text{Ba} \rightarrow \text{Ba}[6s5d(^3D_J)] + \text{Ba} \quad k_2^{\text{Ba}} \qquad (2)$$

The average collision cross sections for these deactivation processes have been characterised by Kallenbach and Koch [16,17] for which we may calculate rate constants of $k_1^{\text{He}}(900\text{ K}) = 2.2 \times 10^{-12}$ cm^3 atom^{-1} s^{-1} and $k_2^{\text{Ba}}(900\text{ K}) = 1.7 \times 10^{-9}$ cm^3 atom^{-1} s^{-1}. We may thus apply the principal of detailed balance for the reverse excitation processes and calculate $k_{-1}^{\text{He}}(900\text{ K}) = 2.2 \times 10^{-14}$ cm^3 atom^{-1} s^{-1} and $k_{-2}^{\text{Ba}}(900\text{ K}) = 1.7 \times 10^{-11}$ cm^3 atom^{-1} s^{-1}. Hence using $p_{\text{He}} = 80$ Torr (1 Torr = 133.3 N m^{-2}) and the vapour density [Ba] = 3.8×10^{13} atoms cm^{-3} [34] at $T = 880$ K with the appropriate $T^{1/2}$ adjustment to mean velocities for rate constant calculations, we may calculate the mean time for ^{3}D–^{1}D collisional excitation = $1/\{k_{-1}^{\text{He}}[\text{He}] + k_{-2}^{\text{Ba}}[\text{Ba}]\} = 49.7$ μs. This may be compared with the time scale of the $^1D_2$ decay in Fig. 1(b) (>2 ms) which provides an atomic marker for Ba(^3D_J). Unfortunately, it was not possible to observe the $^3D_1$–$^1S_0$ emission at $\lambda = 1106.9$ nm directly using the long wavelength interference filter ($\lambda = 1111$ nm) and the R632 p.m. tube. This may be contrasted with previous measurements we have reported on the emission from Sr[5s6s($^1S_0$)] → Sr[5s5p($^1P_1$)] + $h\nu$ ($\lambda = 1124.1$ nm) in the time-domain following energy pooling between Sr[5s5p(^3P_J)] + Sr[5s5p(^3P_J)] using this p.m., tube where its sensitivity is low [33]. In that case, the transition was fully allowed ($A_{nm} \approx 10^8$ s^{-1}) [33] unlike the forbidden nature of the emission involved in this instance, weaker by approximately five orders of magnitude. Fast decay profiles (μs) were observed in this system following laser excitation at $\lambda = 553.5$ nm at $\lambda = 1130.3$ nm ($^1P_1$–$^3D_2$) (λ_7, see later) where the emission is reasonably strong $A_{nm} = 1.2 \times 10^5$ s^{-1} [10,22,37]) and demonstrating that the detection system is operational in this long wavelength region.

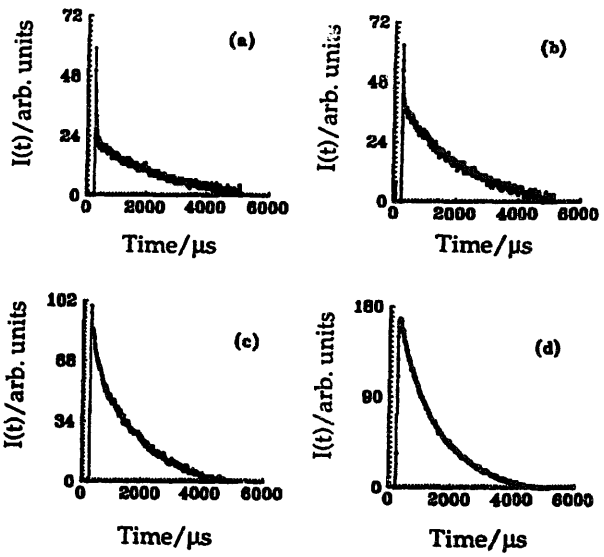

Fig. 2. Examples of the digitised output showing the decay of the time-resolved atomic emission at $\lambda = 791.1$ nm {Ba[6s6p($^3P_1$)] → Ba[6s^2($^1S_0$)]} following the pulsed dye-laser excitation of barium atoms at $\lambda = 553.5$ nm {Ba[6s6p($^1P_1$)] ← Ba[6s^2($^1S_0$)]} in the presence of helium buffer gas ($P_{\text{He}} = 80$ Torr) at various lower elevated temperatures. T/K: (a) 800; (b) 810; (c) 820; (d) 840.

Fig. 2 shows examples of the digitised output at $\lambda = 791.1$ nm {Ba[6s6p($^3P_1$)] → Ba[6s^2($^1S_0$)]} following the pulsed dye-laser excitation of atomic barium at $\lambda = 553.5$ nm {Ba[6s6p($^1P_1$)] ← Ba[6s^2($^1S_0$)]} at different temperatures and hence, varying densities of Ba(6^1S_0). Again there are two components in terms of time regime. The short-time component follows rapid emission ($\tau_c(^3P_1) = 1.2$ μs [23–25]) following fast collisional transfer via the processes [19,20]:

$$\text{Ba}[6s5p(^1P_1)] + \text{He} \rightarrow \text{Ba}[6s6p(^3P_2)] + \text{He} \quad k_3^{\text{He}} \qquad (3)$$

$$\text{Ba}[6s6p(^1P_1)] + \text{Ba} \rightarrow \text{Ba}[6s6p(^3P_2)] + \text{Ba} \quad k_4^{\text{Ba}} \qquad (4)$$

and collisional spin–orbit mixing with Ba(^3P_J) [17]. Breckenridge and Merrow [19] have characterised the collisional cross section for process (3), and Kallenbach and Koch [17], the cross sections for both (3) and (4) whose data we follow as both processes were characterised by the latter workers and noting sensible agreement between both sets of measurements [17,19]. We may readily calculate from the average cross section data of Kallenbach and Koch [17] that, for example, $k_3^{\text{He}}(840\text{ K}) = 8.54 \times 10^{-11}$ cm^3 atom^{-1} s^{-1} and $k_4^{\text{Ba}}(840\text{ K}) = 5.07 \times 10^{-9}$ cm^3 atom^{-1} s^{-1}. Hence for $p_{\text{He}} = 80$ Torr and the vapour density of Ba[$^1S_0$] at this tem-

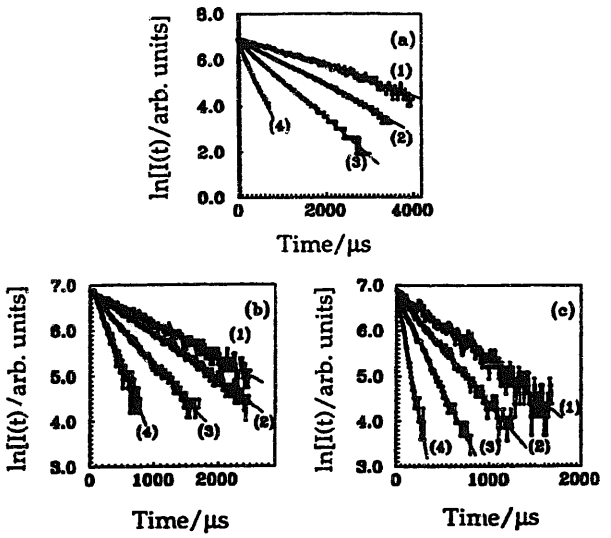

Fig. 3. Examples of the computerised fitting of the normalised digitised output indicating the first-order decay of the time-resolved atomic emission in the long time regime: (a) $\lambda = 791.1$ nm {Ba[6s6p($^3P_1$)] → Ba[6s^2($^1S_0$)]} T/K: (1) 820 (2) 860 (3) 900 (4) 960; (b) $\lambda = 877.4$ nm {Ba[6s5d($^1D_2$)] → Ba[6s^2($^1S_0$)]} T/K: (1) 840 (2) 860 (3) 900 (4) 940; (c) $\lambda = 553.5$ nm {Ba[6s6p($^1P_1$)] → Ba[6s^2($^1S_0$)]}, T/K: (1) 820, (2) 860, (3) 900, (4) 960; following the pulsed dye-laser excitation of barium atoms at $\lambda = 553.5$ nm {Ba[6s6p($^1P_1$)] ← Ba[6s^2($^1S_0$)]} in the presence of helium buffer gas ($P_{He} = 80$ Torr).

perature (1.31×10^{13} atoms cm^{-3} [34]) we may calculate the collisional relaxation of Ba($^1P_1$) to Ba($^3P_2$) = $1/\{k_3^{He}[He] + k_4^{Ba}[Ba]\} = 1.3 \times 10^{-8}$ s, namely, instantaneously. Thus, the long wavelength component (Fig. 2) for emission at $\lambda = 791.1$ nm thus monitors a long-lived precursor, namely, Ba(^3D_J). Following the analogous calculation given above for Ba($^1D_2$), namely, employing the cross sectional data for collisional relaxation of Ba(^3P_J) by He and Ba($^1S_0$) to Ba(^3D_J) given by Kallenbach and Koch [17], we may calculate rate constants for the excitation processes:

$$Ba[6s5d(^3D_J)] + He \rightarrow Ba[6s6p(^3P_J)] + He \quad k_{-5}^{He} \qquad (5)$$

$$Ba[6s5d(^3D_J)] + Ba \rightarrow Ba[6s6p(^3P_J)] + Ba \quad k_{-6}^{Ba} \qquad (6)$$

using detailed balance, namely, $k_{-5}^{He}(900\ K) = 1.7 \times 10^{-15}$ cm^3 atoms^{-1} s^{-1} and $k_{-6}^{Ba}(900\ K) = 10.0 \times 10^{-11}$ cm^3 atoms^{-1} s^{-1}. Hence, for this temperature and $p_{He} = 80$ Torr, $1/\{k_{-5}^{He}[He] + k_{-6}^{Ba}[Ba]\} = 132$ μs. The increasing role of [Ba] can be seen from the increase in the long-time component of the emission at $\lambda = 791.1$ nm with temperature (Fig. 2).

Fig. 3 shows the first-order decay profiles constructed from the normalised digitised output for the long-time emissions at $\lambda = 791.1$ nm {Ba[6s6p($^3P_1$)] → Ba[6s^2($^1S_0$)]}, $\lambda = 877.4$ nm {Ba[6s5d($^1D_2$)] → Ba[6s^2($^1S_0$)]} and $\lambda = 553.5$ nm {Ba[6s6p($^1P_1$)] → Ba[6s^2($^1S_0$)]} following excitation at $\lambda = 553.5$ nm at different temperature. All decay profiles show good first-order behaviour, the former two emissions providing spectroscopic markers for Ba(^3D_J) via collisional excitation to the emitting states, and the third, energy pooling between Ba(^3D_J) + Ba(^3D_J). The increase in the first-order decay coefficients with temperature reflects the increasing role of collisional quenching of Ba(^3D_J) by Ba($^1S_0$) itself whose density varies from 7.42×10^{12} atoms cm^{-3} (820 K) to 2.34×10^{14} atoms cm^{-3} (960 K) [34]. This matter of the vapour pressure data of barium is critical to consideration of the rate data that have been reported for the quenching of Ba(^3D_J) by Ba($^1S_0$).

Whitkop and Wiesenfeld [27] report the rate constant for the collisional quenching of Ba(^3D_J) by Ba($^1S_0$) as $k(Ba^3D_J + Ba, T \approx 730\ K) = (1.9 \pm 0.2) \times 10^{-9}$ cm^3 atom^{-1} s^{-1}. This large quenching constant reflects the use of the early vapour pressure for Ba data employed at that time [27]. More recent vapour pressure data [38] gives values for [Ba] greater by a factor of ca. 15 in the range employed by Whitkop and Wiesenfeld [27] and would increase their rate constant to $k(Ba^3D_J + Ba, T \approx 730\ K) = 1.3 \times 10^{-10}$ cm^3 atom^{-1} s^{-1}. Carlsten [39] has studied the decay coefficient of Ba(^3D_J) versus [Ba] for the temperature range 900–1150 K using a flash lamp absorption technique following laser excitation. The gradient of the plot as given in the paper [39] would yield an average value of $k(Ba^3D_J + Ba) = 1.7 \times 10^{-10}$ cm^3 atom^{-1} s^{-1} for that temperature range. That work employed the vapour pressure data of Hinnov and Ohlendorf [40]. If these data [39] were modified using the later vapour pressure data [38], this would yield $k(Ba^3D_J + Ba) = 3.9 \times 10^{-11}$ cm^3 atom^{-1} s^{-1}. The recent value reported by Vlada et al. [41] is given by $k(Ba^3D_J + Ba, T = 850\ K) = 5.1 \times 10^{-11}$ cm^3 atom^{-1} s^{-1}. We may estimate $k(Ba^3D_J + Ba, T = 900\ K) \approx 2 \times 10^{-11}$ cm^3 atom^{-1} s^{-1} from the combined data in Fig. 3.

The form of Fig. 3 coupled with the calculations on collisional excitation mechanisms indicate that the emission intensities at $\lambda = 791.1$ nm {Ba[6s6p($^3P_1$)] → Ba[6s^2($^1S_0$)]} and $\lambda = 877.4$ nm {Ba[6s5d($^1D_2$)] → Ba[6s^2($^1S_0$)]} are spectroscopic markers for Ba[6s5d(^3D_J)] which follow the exponential decay:

$$Ba[6s5d(^3D_J)]_t = Ba[6s5d(^3D_J)]_{t=0} \exp(-k't) \qquad (i)$$

where the first-order decay coefficient for Ba(^3D_J) can be written as

$$k' = k'_{cm} + \beta/p_{He} + \sum k_Q[Q] \qquad (ii)$$

where k'_{cm} will be dominated by electric dipole-allowed emission from Ba[6s5d($^3D_1$)] in (j,j) coupling. Rapid Boltzmann equilibration between the ^3D_J levels will be established in the present system in the long-time regime [18] where we may describe the equilibrium constants connecting these as $^3D_1 \rightleftharpoons {}^3D_2$ ($\Delta\varepsilon = 182$ cm^{-1} [5,18]) K_1, and $^3D_2 \rightleftharpoons {}^3D_3$ ($\Delta\varepsilon = 381$ cm^{-1}) K_2. Assuming emission from this state is then dominated by the electric dipole-allowed transition $^3D_1 \rightarrow {}^1S_0$ (A_{nm}), we may readily show that k'_{cm} is given by

$$k'_{cm} = A_{nm}/(1 + K_1 + K_1K_2) \qquad (iii)$$

where $F = (1 + K_1 + K_1K_2)$ may be readily calculated by statistical thermodynamics taking the values of 3.05 at 800 K,

3.32 at 1000 K and 5 at infinite temperature where it is solely dependent on statistical weights of the spin–orbit components. We may note immediately that the weak emission at $\lambda = 877.4$ nm {Ba[6s5d($^1D_2$)] → Ba[6s^2($^1S_0$)]} and which required the use of an interference filter is not electric-dipole allowed ($\Delta J = 2$) and only magnetic-dipole allowed in (jj) coupling and is presumably strengthened by collision induced emission. Both the $^3P_1$ and $^1D_2$ states have been shown to act as spectroscopic markers of Ba(^3D_J). The term in β/p_{He} describes diffusional loss and $\Sigma k_Q[Q]$, collisional losses of Ba(^3D_J), including excitation to higher states. The diffusional loss term is relatively small and differences in effective boundary conditions to the diffusion equation from the use of a monochromator system at wide slit width ($\lambda = 791.1$ nm) and an interference filter ($\lambda = 877.4$ nm) will not be large (see later). The emission intensity for states arising from collisional excitation from Ba(^3D_J) such as Ba[6s6p($^3P_1$)] will take the form:

$$I_{em}(791.1\text{ nm}) = GS\{k^{He}_{-5}[He] + k^{Ba}_{-6}[Ba]\}Ba[6s5d(^3D_J)]_{t=0}\exp(-k't) \quad \text{(iv)}$$

where G is the gain of the appropriate photomultiplier which is a function of voltage and S is the sensitivity of the optical system. All emission intensities can, of course, be normalised to a common relative scale. Similar considerations will apply to $I_{em}(877.4\text{ nm})$.

The emission intensity at $\lambda = 553.5$ nm {Ba[6s6p($^1P_1$)] → Ba[6s^2($^1S_0$)]} in the long-time regime following initial excitation at $\lambda = 553.5$ nm arises from energy pooling:

$$Ba[6s5d(^3D_J)] + Ba[6s5d(^3D_J)] \rightarrow Ba[6s^2(^1S_0)] + Ba[6s6p(^1P_1)] \quad k_7 \quad (7)$$

for which $\Delta\varepsilon = 654\text{ cm}^{-1}$. This energy pooling process has been studied in detail by Gallagher and co-workers [30] who report a branching ratio of 0.9966 for this collision and a rate constant of $k_7(860\text{ K}) > 8.1\times10^{-12}\text{ cm}^3\text{ atom}^{-1}\text{ s}^{-1}$. Thus, the intensity of the emission at $\lambda = 553.5$ nm arising from this energy pooling will follow the form:

$$I_{em}(553.5\ nm) = GSk_7Ba[6s5d(^3D_J)]^2_{t=0}\exp(-2k't) \quad \text{(v)}$$

where G and S take the appropriate values for the conditions of p.m. voltage and the wavelength employed.

Fig. 4 shows the variation of the integrated atomic intensities with temperature at $\lambda = 553.5$ nm and 791.1 nm. Whilst the former arises from energy pooling with two Ba(^3D_J) atoms and the latter from energy transfer from Ba(^3D_J), both originate from initial excitation to Ba($^1P_1$), however, they reflect the effective initial yields of Ba(^3D_J) after the optical and collisional relaxation processes that have been presented earlier. This is to be contrasted with an initial yield of Ba($^1P_1$). Simple considerations of attenuation of the dye-laser beam at $\lambda = 553.5$ nm by Ba($^1S_0$) in the reactor would indicate an optimum concentration given by $c = 1/\langle\sigma\rangle l$ to

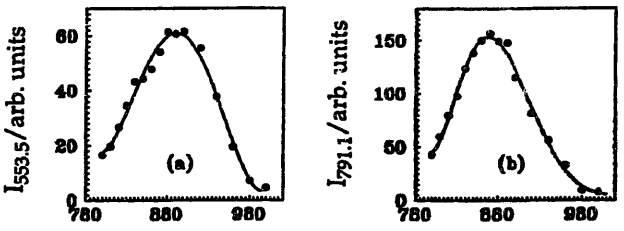

Fig. 4. Variation of the integrated atomic emission intensities with temperature at (a) $\lambda = 553.5$ nm {Ba[6s6p($^1P_1$)] → Ba[6s^2($^1S_0$)]} and (b) $\lambda = 791.1$ nm {Ba[6s6p($^3P_1$)] → Ba[6s^2($^1S_0$)]} following the pulsed dye-laser excitation of barium atoms at $\lambda = 553.5$ nm {Ba[6s6p($^1P_1$)] ← Ba[6s^2($^1S_0$)]} in the presence of helium buffer gas ($P_{He} = 80$ Torr).

yield Ba($^1P_1$) where l is the effective distance from the entrance window into the centre of the reactor (ca. 3 cm). $\langle\sigma\rangle$ is an effective absorption cross section based on a Doppler line shape for the transition Ba[6s6p($^1P_1$)] → Ba[6s^2($^1S_0$)], $\tau_e = (8.37 \pm 0.38$ ns [10]). This would correspond to a low vapour density of Ba($^1S_0$) for a temperature of ca. 600 K. This is clearly not the case here (Fig. 4), partly on account of the large effect of radiation trapping for a transition of this short lifetime. The maxima demonstrate the overall transfer efficiency from Ba($^1P_1$) to Ba(^3D_J) for the long-time integrated atomic emission intensities. The decline at higher temperature reflects collisional quenching of Ba(^3D_J) by the ground state.

$$Ba[6s5d(^3D_J)] + Ba[6s^2(^1S_0)] \rightarrow 2Ba[6s^2(^1S_0)] \quad k_8 \quad (8)$$

The data of Kallenbach and Koch [17] for the quenching of Ba(^3P) to Ba(^3D), coupled with the principle of detailed balance, may be used to calculate the rate data for the excitation processes (see earlier)

$$Ba[6s5d(^3D_J)] + Ba[6s^2(^1S_0)] \rightarrow Ba[6s6p(^3P_J)] + Ba[6s^2(^1S_0)] \quad k_9 \quad (9)$$

$$Ba[6s5d(^3D_J)] + Ba[6s^2(^1S_0)] \rightarrow Ba[6s5d(^1D_2)] + Ba[6s^2(^1S_0)] \quad k_{10} \quad (10)$$

where $k_9(900\text{ K}) = 9.98\times10^{-12}\text{ cm}^3\text{ atom}^{-1}\text{ s}^{-1}$ and $k_{10}(900\text{ K}) = 1.73\times10^{-11}\text{ cm}^3\text{ atom}^{-1}\text{ s}^{-1}$ where $(k_9 + k_{10}) = 2.7\times10^{-11}\text{ cm}^3\text{ atom}^{-1}\text{ s}^{-1}$. This calculation and the quenching data reported here and hitherto [27,39,41] supports, in the main, the removal of Ba(^3D) by Ba($^1S_0$) collisional excitation to the higher lying ^3P and ^1D states.

Fig. 5 shows the variation of the integrated atomic emission intensities with laser energy at $\lambda = 553.5$ nm {Ba[6s6p($^1P_1$)] → Ba[6s^2($^1S_0$)]}, $\lambda = 791.1$ nm {Ba[6s6p($^3P_1$)] → Ba[6s^2($^1S_0$)]} and $\lambda = 877.4$ nm {Ba[6s5d($^1D_2$)] → Ba[6s^2($^1S_0$)]} following excitation at $\lambda = 553.5$ nm. The integrated intensity arising from energy pooling ($\lambda = 553.5$ nm) depending on the integrated form of Eq. (v) and dependent on Ba[6s5d(^3D_J)]$^2_{t=0}$ should at least demonstrate an upward curvature with laser energy; those

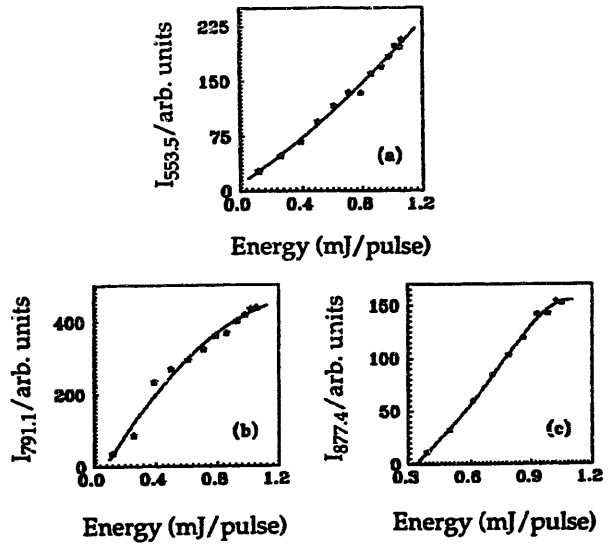

Fig. 5. Variation of the integrated atomic emission intensities with laser energy at (a) $\lambda = 553.5$ nm {Ba[6s6p($^1P_1$)] → Ba[6s^2($^1S_0$)]}, (b) $\lambda = 791.1$ nm {Ba[6s6p($^3P_1$)] → Ba[6s^2($^1S_0$)]} and (c) $\lambda = 877.4$ nm {Ba[6s5d($^1D_2$)] → Ba[6s^2($^1S_0$)] following the pulsed dye-laser excitation of barium atoms at $\lambda = 553.5$ nm {Ba[6s6p($^1P_1$)] ← Ba[6s^2($^1S_0$)]} in the presence of helium buffer gas ($P_{He} = 80$ Torr, 8.6×10^{17} atoms cm^{-3}) at elevated temperature ($T = 900$ K).

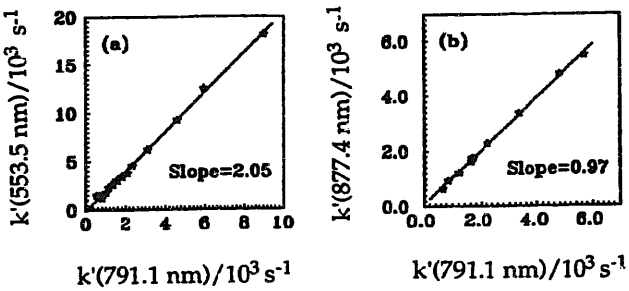

Fig. 6. Comparison of the first-order rate coefficients, k', derived from the intensity profiles for the decay at (a) $\lambda = 553.5$ nm {Ba[6s6p($^1P_1$)] → Ba[6s^2($^1S_0$)]} and (b) $\lambda = 877.4$ nm {Ba[6s5d($^1D_2$)] → Ba[6s^2($^1S_0$)] with that at $\lambda = 791.1$ nm {Ba[6s6p($^3P_1$)] → Ba[6s^2($^1S_0$)]} following the pulsed dye-laser excitation of barium atoms at $\lambda = 553.5$ nm {Ba[6s6p($^1P_1$)] ← Ba[6s^2($^1S_0$)]} in the presence of helium buffer gas in the presence of helium buffer gas ($P_{He} = 80$ Torr) at elevated temperature ($T = 800$–980 K).

dependent on collisional excitation of Ba(^3D_J) ($\lambda = 791.1$, $^3P_1$; $\lambda = 877.4$ nm, $^1D_2$) should ideally be linear with laser energy and do, at least, show curvature in the opposite sense to that for energy pooling.

Fig. 6 is consistent with Eqs. (iv) and (v) with the comparison of the first-order decay coefficients for emission from Ba($^1P_1$) ($\lambda = 553.5$ nm), Ba($^3P_1$) ($\lambda = 791.1$ nm) and Ba($^1D_2$) (877.4 nm) being in the ratio of 2:1:1 within experimental error (±5%). The linearity in the plot of k'(877.4 nm) versus k'(791.1 nm) demonstrates the small difference in diffusional loss using an interference filter for optical separation for the former and a monochromator with wide slits (600 μm typically) for the latter (see earlier). A similar comparison can be made with a comparison of integrated atomic emission intensities. Given that Ba($^1P_1$) arises

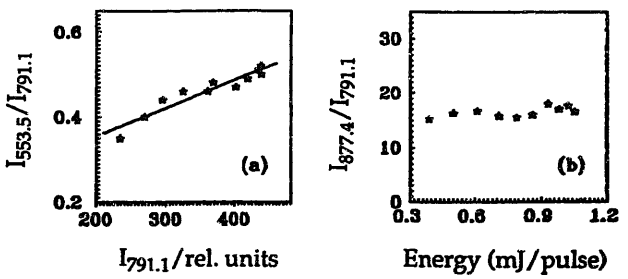

Fig. 7. Variations of the ratios of the integrated atomic emission intensities (I) for (a) $\lambda = 553.5$ nm {Ba[6s6p($^1P_1$)] → Ba[6s^2($^1S_0$)]}/$\lambda = 791.1$ nm {Ba[6s6p($^3P_1$)] → Ba[6s^2($^1S_0$)]} and (b) $\lambda = 877.4$ nm {Ba[6s5d($^1D_2$)] → Ba[6s^2($^1S_0$)]}/$\lambda = 791.1$ nm {Ba[6s6p($^3P_1$)] → Ba[6s^2($^1S_0$)]} with laser energy following the pulsed dye-laser excitation of barium atoms at $\lambda = 553.5$ nm {Ba[6s6p($^1P_1$)] ← Ba[6s^2($^1S_0$)]} in the presence of helium buffer gas ($P_{He} = 80$ Torr, 8.6×10^{17} atoms cm^{-3}) at elevated temperature ($T = 900$ K).

from bimolecular energy pooling between two Ba(^3D_J) atoms whereas Ba(^3P_J) and Ba($^1D_2$) involve a linear dependence on [Ba(^3D_J)], the ratio of the integrated atomic intensities $I_{553.5\text{ nm}}/I_{791.1\text{ nm}}$ should be linearly dependent on $I_{791.1\text{ nm}}$ as seen (Fig. 7(a)) and the ratio $I_{877.4\text{ nm}}/I_{791.1\text{ nm}}$ should independent of laser energy (Fig. 7(b)) as excitation to the emitting states is linear in [Ba(^3D_J)] in both cases (see earlier).

Fig. 8 summarises the conclusions of this investigation. Resonance fluorescence is seen in the short-time domain following direct laser excitation Ba[6s6p($^1P_1$)] at $\lambda = 553.5$ nm with subsequent weak emission from this state in the long-time regime and arising from energy pooling. The details of various aspects of the collisional mechanisms that lead to the long-lived states are described in this paper. Inevitably, the main initial sink of the initial electronic excitation before the long decay processes proceed is the ^3D_J state. Various transitions are listed in Fig. 8. It is clear that Ba[6s5d(^3D_J)] cannot be excited directly but the indirect routes are seen to be relatively efficient given the efficient initial pumping at $\lambda = 553.5$ nm. Thus, the yield of Ba(^3D_J) by emission from Ba($^1P_1$) [10,22]

$$\mathrm{Ba[6s6p(^1P_1)] \rightarrow Ba[6s5d(^3D_2)] + h\nu}$$

($\lambda = 1130.3$ nm, $A_{nm} = 1.2 \times 10^5$ s^{-1})

$$\mathrm{Ba[6s6p(^1P_1)] \rightarrow Ba[6s5d(^3D_1)] + h\nu}$$

($\lambda = 1107.6$ nm, $A_{nm} = 1.2 \times 10^3$ s^{-1})

will be relatively high by this route alone apart from collisional processes. Radiative transfer into Ba(^3D_J) following collisional quenching of Ba[6s6p($^1P_1$)] into Ba[6s6p($^3P_2$)] [19,20] is also relatively efficient as seen from inspection of the Einstein coefficients for emission from Ba($^3P_2$) into Ba($^3D_{1,2,3}$) as well as those for Ba($^1P_1$) into Ba($^3D_{1,2}$) [10,22]. The combination of the Einstein coefficients for excitation into Ba($^1P_1$) coupled with collisional and optical and collisional relaxation into Ba(^3D_J) is thus efficient by comparison with direct optical excitation into the low lying states of Ma, Ca and Sr [3,4]. The present work has shown

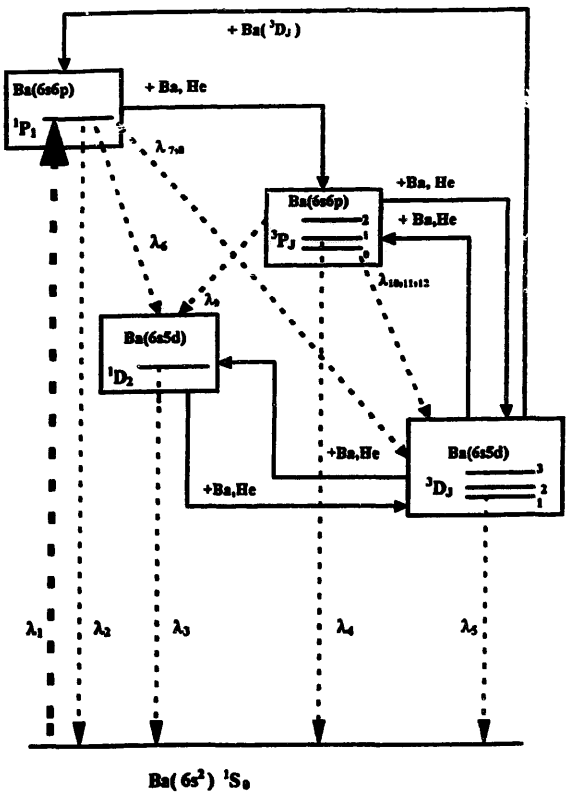

Fig. 8. Excitation and transfer processeses undergone by atomic barium following the pulsed dye-laser excitation of ground state barium atoms at $\lambda = 553.5$ nm {Ba[6s6p($^1P_1$)] ← Ba[6s^2($^1S_0$)]} in the presence of helium buffer gas at elevated temperature. $\lambda_1 = 553.5$ nm, $\lambda_2 = 553.5$ nm, $\lambda_3 = 887.4$ nm, $\lambda_4 = 791.1$ nm, $\lambda_5 = 1106.9$ nm, $\lambda_6 = 1500.0$ nm, $\lambda_7 = 1130.3$ nm, $\lambda_8 = 1107.6$ nm, $\lambda_9 = 4717.1$ nm, $\lambda_{10} = 2551.5$ nm, $\lambda_{11} = 2325.4$ nm, $\lambda_{12} = 2231.2$ nm.

that time-resolved emission using both the decay profiles and the integrated atomic emission intensities from Ba[6s6p($^3P_1$)] and Ba[6s5d($^1D_2$)] in the long time-domain resulting from collisional excitation, and that from Ba[6s6p($^1P_1$)], resulting from energy pooling, may be all used as spectroscopic markers for Ba[6s5d(^3D_J)] which is not directly accessible by laser excitation.

Acknowledgements

We thank the Cambridge Overseas Scholarship Trustees for a Research Studentship held by J.L. during the tenure of which this work was carried out. J.L also thanks the O.R.S. for an award. We also thank the E.P.S.R.C. of Great Britain for the initial purchase of the laser system and a Research Studentship held by one of us (S.A.). Finally, we are also indebted to Dr George Jones of the DRA (Fort Halstead) for encouragement and helpful discussions.

References

[1] W.H. Breckenridge and H. Umemoto, in K.P. Lawley (ed.), *Dynamics of the Excited State, Adv. Chem. Phys.*, Vol. L, Wiley, London, 1982, Chapter 5, p. 325.
[2] W.H. Breckenridge, in A. Fontijn and M.A.A. Clyne (eds.), *Reactions of Small Transient Species: Kinetics and Energetics*, Academic Press, London, 1983, Chapter 4, p. 157.
[3] D. Husain and G. Roberts, Bimolecular collisions involving electronically excited alkaline earth atoms, chapter in J.E. Baggott and M.N.R. Ashfold (eds.), *Gas Phase Bimolecular Processes*, Royal Society of Chemistry, London, 1989, Chapter 6, p. 263.
[4] D. Husain, *J. Chem. Soc. Faraday Trans. 2, 85* (1989) 85.
[5] C.E. Moore, *Atomic Energy Levels*, Nat. Bur. Stand. Ref. Data Ser., Nat. Bur. Stand. Monograph, 35, Vols. I–III, US Government Printing Office, Washington, DC, 1971.
[6] R.W. Solarz and S.A. Johnson, *J. Chem. Phys., 70* (1979) 3592
[7] S.G. Schmelling, *Phys. Rev. A, 9* (1974) 1097.
[8] J.D. Eversole and N. Djeu, *J. Chem. Phys., 71* (1979) 148.
[9] D. Husain and G. Roberts, *Chem. Phys., 127* (1988) 203.
[10] S. Niggli and M.C.E. Huber, *Phys. Rev. A, 35* (1987) 2908.
[11] H.A. Bachor and M. Kock, *J. Phys. B., At. Mol. Phys., 14* (1981) 2793.
[12] J.L. Bowen and A.P. Thorne, *J. Phys. B., Atom. Mol. Phys., 18* (1985) 35.
[13] A. Kallenbach, M. Günther, R. Künnemeyer and M. Kock, *J. Phys. B., Atom. Mol. Phys., 19* (1986) 2645.
[14] E.G. Myers, C.J. Bell, P.G. Pappas and D.E. Murnick, *Phys. Rev. A, 33* (1986) 2798.
[15] D.A. Lewis, J. Kumar, M.A. Finn and G.W. Greenlees, *Phys. Rev. A, 35*(1987) 131.
[16] A. Kallenbach and M Koch, *J. Phys. B., At. Mol. Phys., 22* (1989) 1691.
[17] A. Kallenbach and M. Koch, *J. Phys. B., At. Mol. Phys., 22* (1989) 1705.
[18] E. Ehrlacher and J. Huennekens, *Phys. Rev. A, 50* (1994) 4786.
[19] W.H. Breckenridge and C.N. Merrow, *J. Chem. Phys., 88* (1987) 2329.
[20] J.P. Visticot, P. de Pujo, O. Sublemontier, A.J. Bell, J. Cuvellier, T. Gustavson, A. Lallement, J.M. Mestdagh and A.G. Suits, *Phys. Rev. A, 45* (1992) 6371.
[21] J.P. Visticot, J. Berlande, J. Cuvellier, J.M. Mestdagh, P. de Pujo, O. Sublemontier, A.J. Bell and J.G. Frey, *J. Chem. Phys., 93* (1990) 5354.
[22] P. Hafner and W.H.E. Schwarz, *J. Phys. B., At. Mol. Phys., 11* (1978) 2975.
[23] C.W. Bauschlicher Jr., R.L. Jaffe, S.R. Langhoff, F.G. Mascarello and H. Partridge, *J. Phys. B., 18* (1985) 2147.
[24] J. Reader, C.H. Corliss, W.L. Wiese and G.A. Martin, *Wavelengths and Transition Probabilities for Atoms and Atomic Ions*, Nat. Bur. Stand. Ref. Data Ser., Nat. Bur. Stand. Monograph 68, US Government Printing Office, Washington, DC, 1980, p. 367.
[25] B.M. Miles and W.L. Wiese, *Critically Evaluated Transition Probabilities for Ba I and II*, Nat. Bur. Stand. Technical Note 474, US Government Printing Office, Washington, DC, 1969.
[26] C. Hradecny, J. Slovak, T. Tethal, J.M. Yermolayev and E.V. Podivilov, *Phys. Rev. A, 51* (1995) 3374.
[27] P.G. Whitkop and J.R. Wiesenfeld, *J. Chem. Phys., 72* (1980) 1297.
[28] J.W. Cox and P.J. Dagdigian, *J. Chem. Phys., 79* (1983) 5351.
[29] M.L. Campbell and P.J. Dagdigian, *J. Chem. Phys., 85* (1986) 4453.
[30] J.A. Neuman, A. Gallagher and J. Cooper, *Phys. Rev. A., 50* (1994) 1292.
[31] S. Antrobus, S.A. Carl, D. Husain, Jie Lei, F. Castaño and M.N. Sanchez Rayo, *Ber. Bunsen. Ges. Phys. Chem., 99* (1995) 127.

[32] D. Husain and Jie Lei, *J. Chem. Soc. Faraday Trans., 91* (1995) 811.
[33] S. Antrobus, D. Husain and Jie Lei, *J. Photochem. Photobiol. A: Chem., 103* (1997) 11–17.
[34] D.R. Lide and H.P.R. Frederiske (eds.), *CRC Handbook of Physics and Chemistry* CRC Press, Boca Raton, FL, 75th edn., 1994, pp. 4–124.
[35] *E.M.I. Catalogue*, E.M.I. Publications, 1979.
[36] W.H. Wing and T.M. Sanders, Jr., *Rev. Sci. Instrum., 38* (1967) 1341.
[37] D.R. Lide and H.P.R. Frederiske (eds.), *CRC Handbook of Physics and Chemistry*, CRC Press, Boca Raton, FL, 75th edn., 1994); J.R. Fuhr and W.L. Wiese, *Atomic Transition Probabilities*, 10, p. 134.)
[38] C.B. Alcock, V.P. Itkin and M.K. Harrigan, *Can. Metall. Q., 23* (1984) 309.
[39] J.L. Carlsten, *J. Phys. B., Atom. Molec. Phys., 7* (1974) 1620.
[40] E. Hinnov and W. Ohlendorf, *J. Chem. Phys., 50* (1969) 3005.
[41] C. Vadla, K. Niemax, V. Horatic and R. Beuc, *Z. Phys. D., 34* (1995) 171.